

Computer Vision-based Adaptive Control for Back Exoskeleton Performance Optimization

Andrea Dal Prete^{1,2}, Seyram Ofori², Chan Yon Sin³, Ashwin Narayan², Francesco Braghin¹,
Marta Gandolla¹, and Haoyong Yu²

Abstract—Back exoskeletons can reduce musculoskeletal strain, but their effectiveness depends on support modulation and adaptive control. This study addresses two challenges: defining optimal support strategies and developing adaptive control based on payload estimation. We introduce an optimization space based on muscle activity reduction, perceived discomfort, and user preference, constructing functions to identify optimal strategies. Experiments with 12 subjects revealed optimal operating regions, highlighting the need for dynamic modulation. Based on these insights, we developed a vision-based adaptive control pipeline that estimates payloads in real-time by enhancing exoskeleton contextual understanding, minimising latency and enabling support adaptation within the defined optimisation space. Validation with 12 more subjects showed over 80% accuracy and improvements across all metrics. Compared to static control, adaptive modulation reduced peak back muscle activation by up to 23% while preserving user preference and minimising discomfort. These findings validate the proposed framework and highlight the potential of intelligent, context-aware control in industrial exoskeletons.

Index Terms—Back exoskeleton, computer vision, exoskeleton optimization, deep learning, context awareness

I. INTRODUCTION

Musculoskeletal disorders are a growing concern in industrial workplaces, where workers in construction sites, production, logistics, and others who regularly lift heavy loads face significant risks. To address these issues, back support exoskeletons (BEs) have been developed, aiming to reduce muscular activation and spinal loadskey contributors to back impairment [1]–[4]. Over the past few decades, advancements in the design of active BEs have improved their kinematic compatibility, reduced their weight, enhanced their acceptability, and proposed innovative designs [5]–[9]. Despite these improvements, challenges remain, particularly in terms of optimization strategies and adaptation, as current BEs lack effective mechanisms to integrate user and environmental data for optimal high-level control, leaving opportunities for significant performance gains untapped [10]. For instance, even though keeping high assistance regardless of the payload could seem a valuable strategy, since increasing the exoskeleton support level can reduce muscular effort, past studies indicate that these benefits plateau at higher support levels [11]. Furthermore, increasing support can lead to joint misalignment, discomfort, and reduced user acceptability, highlighting the

need to balance multiple factors/metrics such as muscular activity, perceived discomfort, and user preference in optimizing exoskeleton performance [12], [13]. Nevertheless, introducing assistance dependencies to the payload introduces even further uncertainties on which is the best support to select. Thus, an important open question in the research deals with selecting optimal support levels based on environmental conditions or user intent to maximize performance. Another key question, in contrast, concerns the exoskeleton’s perception and adaptation capabilities. Notably, adaptive control in response to user intent and environmental factors is feasible only in active exoskeletons, which are increasingly demonstrating their adaptability and effectiveness. In particular, real-time payload estimation and adaptive support modulation have emerged as critical areas of research for enhancing exoskeleton performance [10], [14]. Furthermore, previous research highlights that the highest muscular activation in back muscles occurs during the initial phases of a lifting cycle [15], emphasizing the need for rapid and precise support modulation before the lifting process begins. Existing payload estimation techniques often fail to address this latency issue, limiting their effectiveness. Previous researchers proposed some valuable strategies to exploit exoskeleton adaptation to user needs in the payload estimation and environment comprehension enhancement attempts. One of the first and most straightforward solutions was proposed by Luis A. Mateos [16], which employed force sensing resistor insoles to measure total weight changes due to payload handling, estimate the payload, and distinguish between lifting and lowering phases. Related research by Matijevich *et al.* investigated a sensor network with a minimal number of sensors to accurately estimate low back loads, concluding that pressure insoles are essential for proper back load estimation as they carry crucial information about the payload [17]. Lazzaroni *et al.* [18], [19] and Toxiri *et al.* [20] employed optimized electromyography (EMG)-based armbands to measure muscular contraction while grasping objects and to modulate the exoskeleton support based on grasping strength. While this strategy demonstrated significant potential, subject-specific behaviours, persistent EMG-related drawbacks, and ergonomic considerations (e.g., skin placement requirements) limit its broader applicability. Similarly, Islam *et al.* [21] and Tahir *et al.* [22] proposed force-myography (FMG)-based sensors that correlate muscular volume changes with muscular contraction and payload estimation. Although these methods showed promising results in small-scale tests, they face challenges with output sensitivity to sensor placement and inter- and intra-subject variability, leading to low generalization

¹ Department of Mechanical Engineering, Politecnico di Milano, Italy. ² Department of Biomedical Engineering, National University of Singapore (NUS), Singapore. ³ School of Science and Technology, Singapore University of Social Sciences (SUSS), Singapore.

Corresponding author e-mail: andrea.dalprete@polimi.it.

capabilities [23]. Pesenti *et al.* [24] explored Long Short Term Memory network-based models to classify payload weights using body kinematics obtained from Inertial Measurement Units (IMU) sensors, while other researchers integrated Natural Language Processing (NLP) interfaces into exoskeleton controls to allow user-driven support modulation [25]. However, these approaches suffer from latency issues, with long inference times causing delays in response. As previously noted, the highest muscular activation occurs at the beginning of the lifting cycle, underscoring the need for exoskeletons to provide early-phase support to maximize effectiveness. To address these gaps, this manuscript explores a novel optimization framework for active back exoskeletons, considering payload estimation, muscular activity reduction, user discomfort, and preferences. We present a computer vision-based pipeline that leverages state-of-the-art techniques for object detection, selection, and payload estimation, enabling exoskeletons to operate in high-performance regions of the defined optimization space. Specifically, the contributions of this research include:

- **Optimization space definition.** We formulate a novel optimization space defined by two control variables, payload and assistance level, and conduct a baseline experimental campaign with 12 subjects. Using the collected data, we develop a smooth Performance Optimization Representation Function based on EMG activity reduction, user discomfort, and preference. This framework identifies areas in the optimization space that maximize exoskeleton performance.
- **Vision-based payload estimation pipeline.** Building on the insights from the optimization space analysis, we design a real-time computer vision pipeline to enhance environmental comprehension and payload estimation. The pipeline integrates cutting-edge deep learning models to detect objects, predict payloads, and adapt support levels according to the optimal trends found in baseline experiments.
- **Integration and validation.** We integrate the vision-based pipeline into the exoskeleton control loop and validate its performance through tests involving 12 subjects. The validation includes assessing EMG signals, perceived discomfort, and user preference.
- **Open-source contribution.** To advance the field, we provide open-source data and code as supplementary material for further scientific exploration and development.

This study tackles two key challenges: defining optimal exoskeleton support regions and enabling rapid, subject-independent payload estimation. By addressing these issues, we aim to establish new performance benchmarks for active back exoskeletons in industrial settings while introducing a novel approach to enhance their contextual awareness.

Outline. Section II describes the formulation of the optimization space, the development of the environmental comprehension pipeline, and the hardware used for the experiments. Section III details both baseline and validation experiments with human subject. The results are presented in Section IV and the discussion in Section V. Section VI draws the conclusions of the paper, while the Supplementary Material

provides technical details on the shared dataset and code.

II. METHODS

A. Exoskeleton Optimization Searching Space

As introduced, in the first part of our research we aim to identify optimal operating regions for back exoskeletons by considering two variables: the assistance level (A_s) and the payload handled by the user (P_{yl}). The former is a controllable parameter, while the latter is determined by the environment, representing the weight of the object chosen by the user. Fig. 3-I illustrates some performance representation functions (J_j) defined within this optimization space, highlighting the exoskeleton's optimal/suboptimal operating regions. To formulate the optimization functions, we conducted experiments with 12 subjects, sampling discrete points in the space as described in section III-A, resulting in a dataset:

$$D = \{x^i, t^i\}_i^N \quad (1)$$

where $x^i = (A_s^i, P_{yl}^i)$ are pairs of assistance and payload levels, and t^i represent samples of the objective function (J_j^i). Using Gaussian Processes (GP) with a Radial Basis Function (RBF) kernel implemented via the GPy library in Python [26], we interpolate D to obtain a smooth, continuous function [27]:

$$J_j(A_s, P_{yl}) = t, \quad J_j: \mathbb{R}^2 \rightarrow \mathbb{R}. \quad (2)$$

The Total Performance Optimization Representation Function (T-ORF) combines three contributions: i) EMG activity reduction optimization representation function (EMG-ORF) $J_{EMG}(A_s, P_{yl})$, ii) perceived discomfort optimization representation function (D-ORF) $J_{dsc}(A_s, P_{yl})$, and iii) user preference optimization representation function (P-ORF) $J_{prf}(A_s, P_{yl})$. During each test (see Section III-A), J_{EMG} measures the percentage reduction in muscular activity when using the exoskeleton compared to no-exoskeleton condition. For J_{dsc} , a questionnaire with the following nine weighted questions ($q_i, i=1, \dots, 9$) assesses discomfort:

- 1) I experience uncomfortable forces compared to other conditions.
- 2) I feel highly comfortable in the current setting.
- 3) I had to work against the assistance in the current setting.
- 4) The exoskeleton restricts my natural movement in the current setting.
- 5) I have to think more about my movements in the current setting.
- 6) I felt nervous and unsafe in the current setting.
- 7) My fatigue is reduced in the current setting.
- 8) I am satisfied with the current setting.
- 9) The exoskeleton is useful for my task in the current setting.

Questions are rated on a scale from 1 (strongly disagree) to 5 (strongly agree). The weighting scheme prioritizes questions that are more directly related to discomfort (i.e., Questions 1, 2, and 4) by assigning them higher weights, while questions with a more indirect connection to discomfort receive lower weights. Specifically, the weights used in the formulation of the discomfort function were as follows: $w_1 = 2$, $w_2 = 2$, $w_3 = 1.5$, $w_4 = 2$, $w_5 = 1$, $w_6 = 1$, $w_7 = 1$, $w_8 = 1$, and $w_9 = 1$.

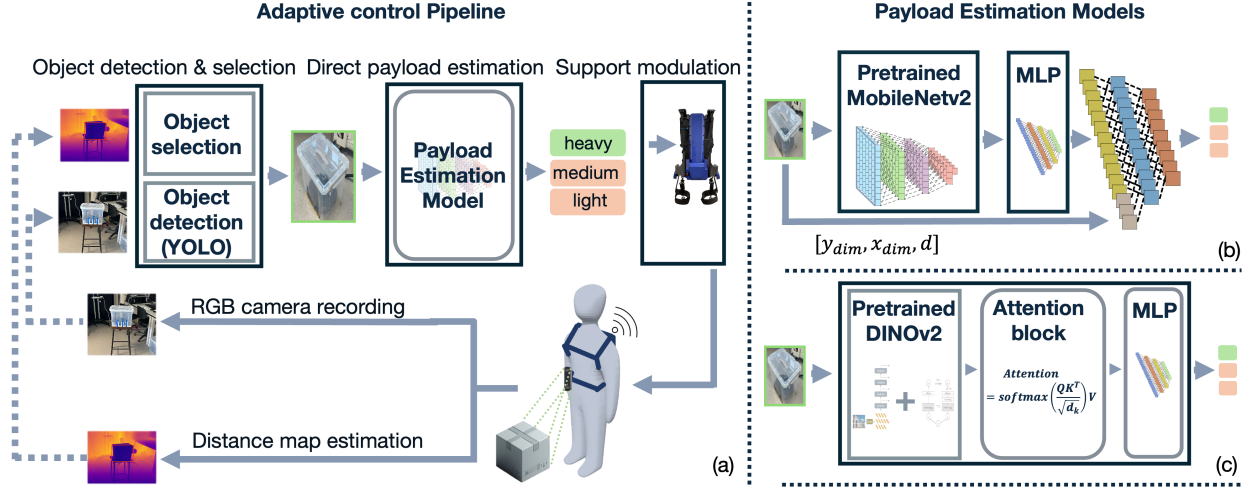


Fig. 1: Outline of the Computer Vision-Based Adaptive Control Pipeline and the architectures of the payload estimation models, where MLP stands for Multilayer Perceptron.

This reflects a deliberate emphasis on the most relevant factors influencing perceived discomfort. With scores flipped for positively framed questions (2, 7, 8, 9). The final sample of the discomfort function is calculated as:

$$J_{dsc}(A_s^i, P_{yl}^i) = \sum_{k=1}^9 w_i q_i. \quad (3)$$

For J_{prf} , subjects indicate their preferred assistance between light and strong when lifting light (5 kg) and heavy (15 kg) weights. After GP interpolation and normalization, the total function is:

$$J_{tot}(A_s, P_{yl}) = 0.6J_{EMG} - 0.2J_{dsc} + 0.2J_{prf}. \quad (4)$$

The J_{EMG} component is weighted higher as it provides a quantitative performance measure, while J_{dsc} and J_{prf} are qualitative. The total function $J_{tot}(A_s, P_{yl})$ reflects the negative cost of operating in a specific region, with higher values indicating better performance. This optimization space guides the selection of assistance levels to maximize overall performance based on muscular activity reduction, perceived discomfort, and user preference.

B. High-Level Control Strategy for BE Optimization

After formulating the optimization space as outlined in section II-A, our results indicate that a static support level cannot maximize performance across all payload conditions. Instead, the back exoskeleton must adapt its control strategy to the payload. To address this, we developed a Computer Vision-based Adaptive Control Pipeline (CVAC) for high-level support adaptation, illustrated in Fig. 1 (a). This pipeline integrates RGB images from an embedded camera for object detection and depth data from a depth sensor for object selection, identifying the most likely object to be picked up by the user. The selected objects image is processed by a fine-tuned Vision Transformer (ViT) [28] to estimate object weight directly, classifying it as light, medium, or heavy. This classification guides the selection of low, medium, or high assistance levels based on the optimization space defined in

section II-A. This work focuses on the general case where the weight of objects (e.g., transparent boxes) is unknown, requiring a deep learning model to infer weight based on object content. The following sections describe each layer of the high-level control pipeline in detail.

1) Object Detection & Selection

The first stage of the pipeline handles object detection and selection. To enhance environmental awareness, we fine-tuned YOLOv11 [29] on a custom dataset to detect transparent boxes, which allows subsequent layers to infer weight from the boxes contents. The dataset comprises 831 images acquired at the BioRobotics Lab at the National University of Singapore (NUS), and labeled with “box” class and bounding box coordinates, split into 88% training, 9% validation, and 3% testing. The fine-tuned YOLO operates on cloud GPUs in real-time, processing RGB frames from the embedded camera. Since YOLO may detect multiple objects, a Time of Flight (ToF) distance map sensor estimates each object’s approximate distance information, which we use to identify the one most likely to be picked up. Although we tested state-of-the-art Monocular Depth Estimation (MDE) models such as DepthAnythingv2 [30] and MiDaS [31] fine-tuned for metric depth estimation (further details in supplementary materials), we opted for the Arducam ToF camera due to its superior performance in indoor environments within our application range ($[0-4]m$). Using the distance map data, we compute a probability factor α_i for each detected object as follows:

$$\alpha_i = 10 \cdot e^{-\lambda_\theta |\theta_i|} \cdot e^{-\lambda_d d_i} \quad (5)$$

where $\lambda_\theta = 0.1$ and $\lambda_d = 0.5$ control decay rates, optimized during preliminary tests, θ_i is the angle of the i -th object in the cameras field of view (with 0 at the center), d_i is the objects distance, and 10 is just a scale factor. Objects farther from the user or closer to the fields boundaries are assigned lower probabilities. After normalizing the factors using softmax, we select the object with the highest pick-up probability as a candidate. If the object with highest probability is within $2m$, we consider the lifting cycle starting soon, we block the recogni-

tion pipeline, we crop the environment image on the bounding box of the candidate object, and pass it to the next layer.

2) Payload Estimation

After the object detection and selection layer (section II-B1), we feed the selected objects cropped image into a fine-tuned deep-learning model for direct weight classification between light, medium, and heavy. For this purpose, we compare two state-of-the-art models: MobileNetv2 [32], a Convolutional Neural Network (CNN) optimized for real-time performance, and DINOv2, a ViT-based foundation model well known for high-quality feature extraction and contextual understanding capabilities [33]–[35].

MobileNetv2 Approach (Fig. 1, b): MobileNetv2 extracts features from input images of shape (256,256,3), outputting (1,8,8,1024) feature maps, which are flattened into 65,536 features. These are mapped to a 32-dimensional space using a four-layer fully connected network. To enhance physical perception, we concatenate physical features (bounding box dimensions and object distance) with the extracted vector, resulting in a 35-dimensional input to a final linear layer for weight classification. We use ReLU activations, softmax for output, RMSprop optimizer ($lr = 1e^{-4}$), and categorical cross-entropy loss. In this case, we only use MobileNetv2 to extract features from images, and we train the layers defined above on the new latent space of extracted features.

DINOv2 Approach (Fig. 1, c): We use DINOv2 pretrained base model available at [36] to process the input image, and we stuck a single-head attention block at the end of it. The output features (1,324,768) are averaged, producing a 768-dimensional vector fed into an MLP with dropout (0.4) and ReLU activation, and softmax for output. Unlike MobileNetv2, because DINOv2 showed strong depth perception capabilities in past research, no physical features are added in this case. We use Adam optimizer ($lr = 1e^{-4}$) and categorical cross-entropy loss. In this case, we fine-tune DINOv2 to our specific classification objective, freezing its core weights while updating the parameters of the last additional layers during training.

In both cases, the models were trained on a dataset of 5480 labeled images (32.03%, 34.01%, and 33.96% distributions for light, medium, and heavy weights) collected at the BioRobotics Lab at the National University of Singapore (NUS). The first model was trained on features from MobileNetv2 for 40 epochs with a batch size of 400, while DINOv2 was fine-tuned for 20 epochs with a batch size of 40. Codes, datasets, and further details on the choice of hyperparameters are provided as supplementary materials.

3) Support Modulation

To modulate the exoskeleton support between low, medium, and strong, we use a simple parameter k_{pyl} to scale the assistive torque provided to the hip joints within a lifting cycle. We find subject-specific values for k_{pyl}^{min} , k_{pyl}^{max} during experiments as explained in section III-A to find the minimum and maximum peak value of assistance which the subject feels comfortable with while lifting a light weight (5 kg) and a heavy weight (15 kg) respectively. Then, we find the k_{pyl}^{medium} as the value at 65% of the $[k_{pyl}^{min}, k_{pyl}^{max}]$ range, according to the optimal trend found and motivated in section IV-A.

C. Hardware

The hardware used is a single-motor back-support exoskeleton (BSE) developed at the National University of Singapore (NUS) [5], shown in Fig. 2 (a). It features a differential series elastic actuator (D-SEA) powered by a 120W servo motor (RMD-L-5015) to deliver lifting assistance, with a nominal assistive torque of 30Nm. The exoskeleton ensures precise force control and active backdrivability, allowing support during lifting while preserving walking autonomy. To enable the CVAC, we use an RGB camera (12MP) and an Arducam Time of Flight (ToF) sensor (240x180 @ 30fps, sub-2cm accuracy), with data acquisition handled by a Raspberry Pi 4B. Aligned with Industry 5.0 principles, we offload the system from the pipeline computational tasks by taking advantage of the cloud. A wireless connection links the exoskeleton to a remote computational station (Apple M3 chip, 8-core CPU, 10-core GPU, 24GB RAM) running the pipeline. After inference, outputs are sent back to the Raspberry Pi to modulate assistance in real-time, achieving an average 100ms inference time (10fps) while offloading deep learning tasks to the cloud.

III. EXPERIMENTS

For both baseline and validation experiments, participants were eligible if they were adults aged 18–65, with a height of 160 – 200 cm, capable of providing informed consent, and in good health to perform weightlifting tasks safely. The experiments took place at the BioRobotics Lab at the National University of Singapore (NUS). A total of 24 male healthy subjects (age: 24.29 ± 2.29 yo; height: 176.04 ± 5.30 cm; weight: 71.98 ± 8.23 kg) voluntarily participated in the experiments, and none of the participants reported having a previous low back injury at the time of data collection. Twelve subjects participated in baseline tests, and 12 took part in validation tests, following recommendations for pilot studies to ensure feasibility, precision, and applicability to future research [37]. The experiment protocol was approved by the NUS Institutional Review Board (IRB) Committee with

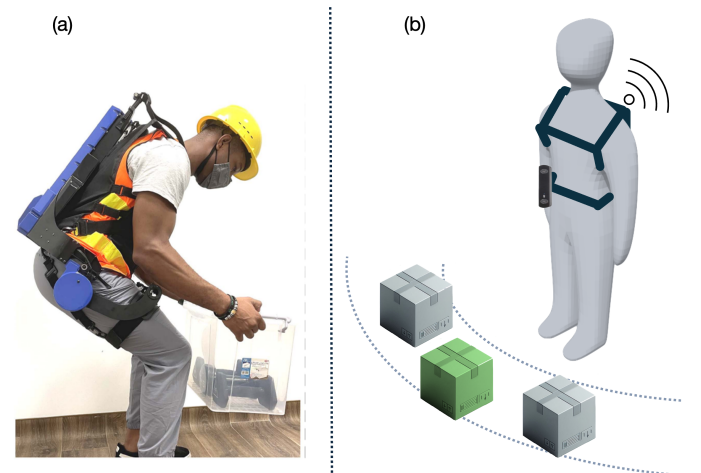


Fig. 2: The back support exoskeleton [5] (a) and validation experiments setting (indoor environment) (b).

Reference Code LH-20-021, and experiments were conducted in accordance with the Research Compliance Policy on Human Subjects and Biomedical Research. Before the study began, the investigators explained the general purpose of the study and obtained verbal and written informed consent from the participants. During all experiments, participants were continuously monitored to ensure safety and avoid accidents. In all experiments, the BSE was utilized in active mode, with muscular activation recorded for the back Erector Spinae Iliocostalis (ESI) and Longissimus (ESL) muscles on both the right and left sides, as well as the leg Biceps Femoris (BF) and Rectus Femoris (RF) muscles. Muscle locations were identified following the SENIAM EMG Placement Guidelines [38]. To standardize data collection, Maximum Voluntary Contraction (MVC) exercises were performed for each muscle, enabling subsequent signal normalization during analysis. EMG signals were recorded using the Delsys Trigno Wireless System (Delsys Inc., Boston, MA, USA) at a 2150 Hz sampling frequency. Data analysis adhered to best practices [39], including the application of a butterworth bandpass filter with low and high cut-off frequencies of 20 Hz and 450 Hz, respectively. Signals were rectified, and the root mean square (RMS) was calculated using a 200 ms sliding time window. For baseline tests, where participants performed tasks in fixed positions, average and peak activation values were analyzed over the entire acquisition period. For validation tests involving walking and lifting, the analysis focused exclusively on lifting cycles. Weights of 5, 10, and 15 kg, also referred to as light weight (LW), medium weight (MW) and heavy weight (HW), were selected for testing based on laboratory equipment availability and safety standards. Three control strategies (low, medium, and strong assistance levels) were used. Preliminary trials were conducted with each participant to calibrate low assistance (LA) and strong assistance (SA) levels based on subjective perception while lifting a 5 kg and 15 kg weight, respectively. For baseline tests, medium assistance (MA) was defined as 50% of the range between LA and SA. For validation tests, medium assistance was set at 65% of this range, as informed by baseline results discussed in Section IV-A.

A. Baseline Experiments

As explained in Section II-A, we conducted experiments with 12 subjects to define a two-dimensional optimization space, identifying the appropriate support level based on the payload, considering muscular activity reduction, perceived discomfort, and user preference as performance metrics. Since we classify weights and support levels into three discrete categories (low, medium, and high), there are nine potential combinations to test the exoskeleton's performance. Additionally, three baseline conditions (LW, MW, and HW) without the exoskeleton bring the total to 12 conditions. To minimize testing time and subject fatigue, we used fractional factorial design [40], reducing the experiments to eight while maintaining statistical significance. This design samples the boundaries, corners, and midpoint of the optimization space and compares them to the no-exoskeleton baseline. For baseline experiments, the subject stands in a fixed position and repetitively lifts a box

of varying weights per condition, first without the exoskeleton and then with different support levels. Each lifting cycle is synchronized to 35 beats per minute (bpm) using a metronome to standardize movement across subjects. A lifting activity consists of seven cycles, lasting a total of 30 seconds. A minimum rest time of 3 minutes is provided between activities to prevent fatigue or injury. Performance metrics were sampled as follows: during preliminary trials, users identified their preferred assistance level (light or strong) for low and heavy weights, yielding samples of $J_{prf}(A_s^i, P_{yl}^i)$. We measured muscular activation in back and leg muscles, as described in Section III, and compared it to non-exoskeleton conditions for the same weight. The percentage reduction in muscular activity provided samples of the EMG-ORF $J_{EMG}(A_s^i, P_{yl}^i)$. After each trial with the exoskeleton, subjects completed a questionnaire to evaluate perceived discomfort for each condition as outlined in Section II-A. The combined ratings from these questions, processed using Equation 3, provided samples for the perceived discomfort representation function $J_{dsc}(A_s^i, P_{yl}^i)$.

B. Pipeline Validation Experiments

For pipeline validation experiments, we designed a dynamic protocol to evaluate the payload estimation pipeline and the exoskeleton's adaptation capabilities in a more variable environment. The subject starts from a fixed position and walks to three boxes placed in fixed positions ahead, containing 5, 10, or 15 kg each, as shown in Figure 2 (b). To enhance generalization, we shuffle the positions and contents of the boxes before each test. The subject approaches each box, lifts it individually, and returns to the starting position. This process is repeated three times, ensuring each box is lifted three times. We performed this protocol under three conditions: without the exoskeleton, with static light support (preselected based on subject characteristics), and with adaptive pipeline control. This setup allows us to compare muscular activity across conditions for each lifting cycle. As validation metrics, first of all, we keep track during the experiment of the pipeline classification outputs and ground truth. In this context, because latency is an important concern, we only consider correct classifications happening before the lifting cycle starts. We also measure reductions in muscular activity targeting the same muscles of Section III-A, by comparing the no-exoskeleton condition with the static and adaptive control conditions. We collect user feedback using the same discomfort questionnaire described in Section II-A, and we gather user preferences between static and adaptive control. This approach enables us to sample the Validation Representation Functions (VRF) $J_{EMG}(A_s^i, P_{yl}^i)$, $J_{dsc}(A_s^i, P_{yl}^i)$, and $J_{prf}(A_s^i, P_{yl}^i)$ for each static/adaptive assistance (StA/AdA) and payload level pairing, creating a final validation space. Using this space, we assess the performance of adaptive control compared to static control.

IV. RESULTS

A. Baseline Experiments - Exoskeleton Optimization Space

1) EMG-ORF

By analyzing the muscular activation data from the experiments in Section III-A, we derive the EMG-ORF

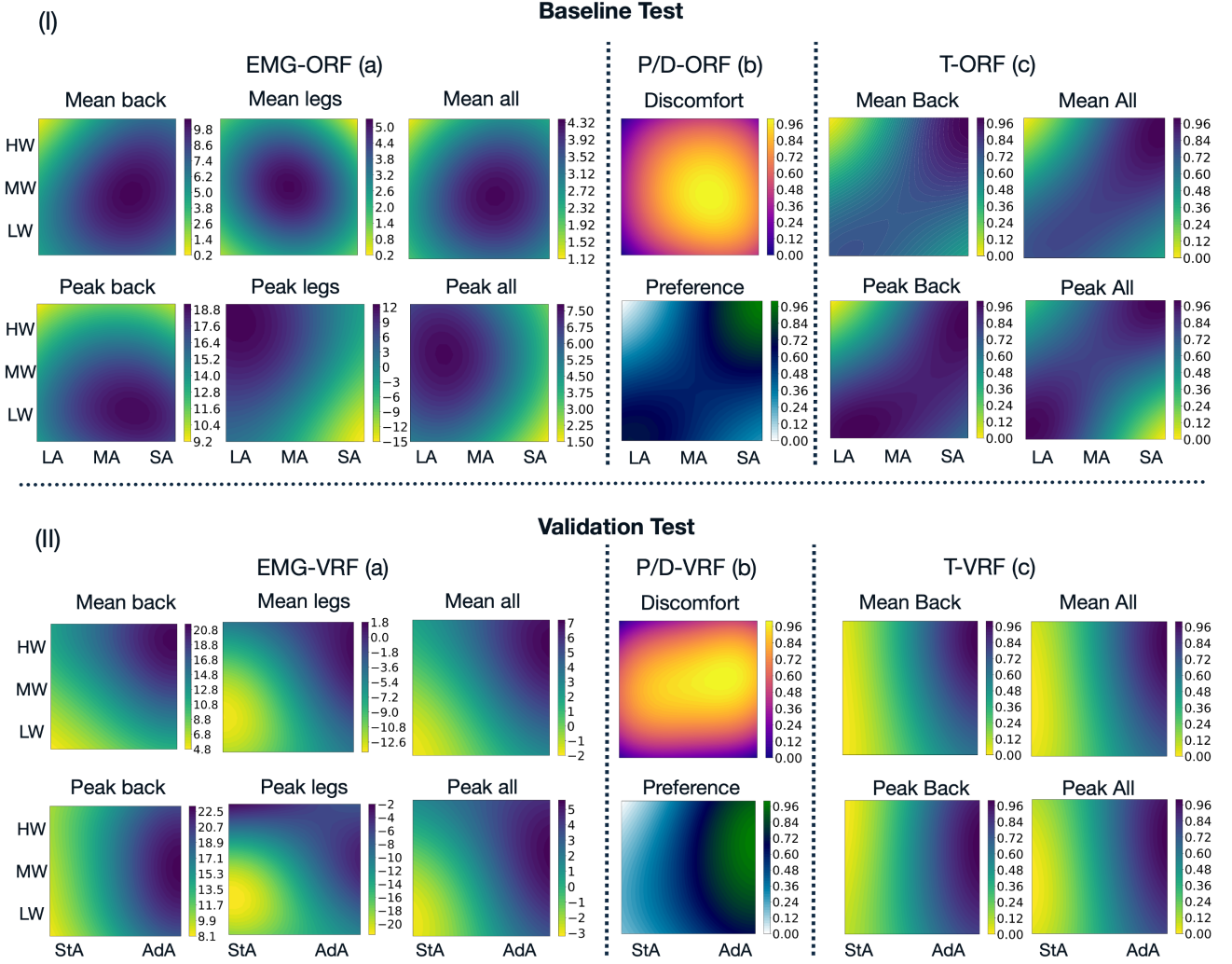


Fig. 3: EMG, Discomfort, Preference, and Total Representation Functions from both Baseline (I) and Validation (II) tests. EMG-ORF (Optimization Representation Functions) and EMG-VRF (Validation Representation Functions) are divided into mean/peak values for back muscles, leg muscles, and total muscle contributions. Similarly, T-ORF and T-VRF are evaluated for each back/all mean/peak combination. For EMG functions, the scale on the right indicates the percentage reduction relative to the no-exoskeleton condition, while for other functions, it represents the normalized value. LW, MW, and HW denote low, medium, and heavy weight conditions. Assistance strategies include LA, MA, and SA for light, medium, and strong assistance in Baseline tests, while StA and AdA refer to static and adaptive assistance in Validation tests.

$J_{EMG}(A_s, P_{yl})$ shown in Figure 3 (I-a). These functions identify optimal performance areas based solely on muscular activity reduction. For instance, reducing back muscle activity consistently requires high assistance, achieving a 6.32% mean and 16.92% peak reduction for low weights, around 9.62% mean and 15.00% peak reduction for medium weights, and a 6.13% mean and a 9.14% peak reduction for high weights. However, high assistance for low weights significantly increases peak activation in leg muscles (-15.00%), which benefit more from medium or light support. The peak EMG-ORF for leg muscles indicates that transitioning diagonally from low-weight light-assistance to high-weight strong-assistance maintains relatively stable peak leg muscle activation while maximizing mean reduction (5.00% mean reduction for medium assistance with medium weight). Overall, considering all muscles together, medium to high assistance is preferable for mean reduction while medium to low for peak. However, given the adverse effect of high

assistance on peak leg muscle activation, a better approach is to use low assistance for low weights and high assistance for high weights. This strategy balances maximizing back muscle activity reduction while minimizing peak activation in the legs.

2) Discomfort & Preference-ORF

As outlined in Section II-A, the discomfort function was sampled by combining the ratings for each question, adjusting for the negative meaning of discomfort by flipping the ratings of positively worded questions. Using Equation 3, we obtained discomfort samples for different (A_s^i, P_{yl}^i) pairs. For user preferences, we collected responses on LA/SA preference for LW/HW scenarios. By fitting these samples with GP, we derived continuous formulations of J_{dsc} and J_{prf} within the optimization space, as shown in Figure 3 (I-b). The results reveal that perceived discomfort peaks for medium weights with medium-to-high support. Overall, low assistance is preferable to minimize discomfort, regardless of the payload. Conversely, user preferences indicate a tendency to favor high assistance

for heavy weights and low assistance for light weights.

3) Total-ORF

It's clear that different ORFs' contributions can be considered individually to select the best assistance for a given payload for a specific metric optimization. In our case, to maximize acceptability and effectiveness, we combine the normalized versions of EMG-ORF, D-ORF, and P-ORF into a T-ORF J_{tot} , considering EMG contributions such as mean and peak reductions in back and overall muscle activity, as shown in Figure 3 (I-c). Results suggest that to optimize EMG reduction, discomfort, and user preference, assistance should be low for light weights and increase with the payload, following a non-linear trend. Based on this, we focus on optimizing "Mean All" activity to minimize muscle activation while avoiding excess leg muscle activation. To determine the optimal assistance for each payload, we compute the partial derivative of J_{tot} with respect to assistance and slice the function along the payload axis. Setting the derivative to zero ($\frac{\partial J_{tot}}{\partial A_s} = f(P_{yl}, A_s) = 0$) for each chosen P_{yl} yields the optimal A_s^{opt} corresponding to each selected P_{yl} , as shown in Figure 4. We then fit the points to an exponential function describing the relationship between payload and optimal support:

$$P_{yl} = a * e^{b * A_s^{opt}} + c \quad (6)$$

with $a=0.72$, $b=1.10$, and $c=-1.20$. This function identifies an optimal region in the assistance-payload space, suggesting that if we had a way to continuously estimate payloads, we'd always be able to select the best-performing assistance in terms of our defined metrics. Following these findings, instead of the midpoint between low and high assistance levels we select 65% assistance during validation for medium weights. We provide in the supplementary materials the a , b , c values found for different EMG contributions.

B. MobileNet2 - DINOv2 comparison

As discussed in Section II-B2, we compared two deep learning models, namely MobileNet2 and DINOv2, primarily used to map input images into meaningful feature spaces. Figure 5-I illustrates the training and validation performance of the two models. Categorizing box weights based on their contents proved challenging, introducing noise into both training processes, particularly due to dataset variability. Nonetheless, the DINOv2-based model demonstrated more

stable, reliable, and less overfitting training compared to MobileNet2-based one, achieving better performance while trained for a lower number of epochs in terms of higher accuracy improving from 90.32% to 94.72% and average precision from 90.23% to 94.83%. We found that these improvements were even more pronounced on other datasets, which we provide in the supplementary materials.

To understand these differences, we analyzed the features extracted by both models. For MobileNet2, we visualized convolutional filters and the activated features during forward passes. For DINOv2, we followed the method in [35], performing PCA on its output features while only keeping the first 3 components and reshaping them into an image-like format ($width, height, channels=3$). Figure 5-II compares a misclassified image from MobileNet2 to the same correctly classified image from DINOv2. While both models identified objects within transparent boxes, MobileNet2 struggled to separate background elements and filter out irrelevant details (e.g., blue tape on the floor and a stack of paper tickets on the

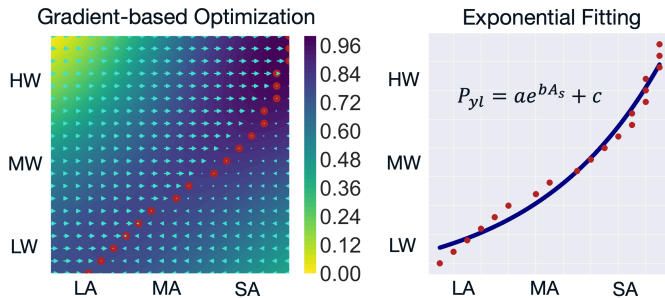


Fig. 4: Gradient-based optimization of J_{tot} and fitting process of the optimization points. Arrows show the direction to follow for performance improvement, with red dots indicating the maximum O-RF values.

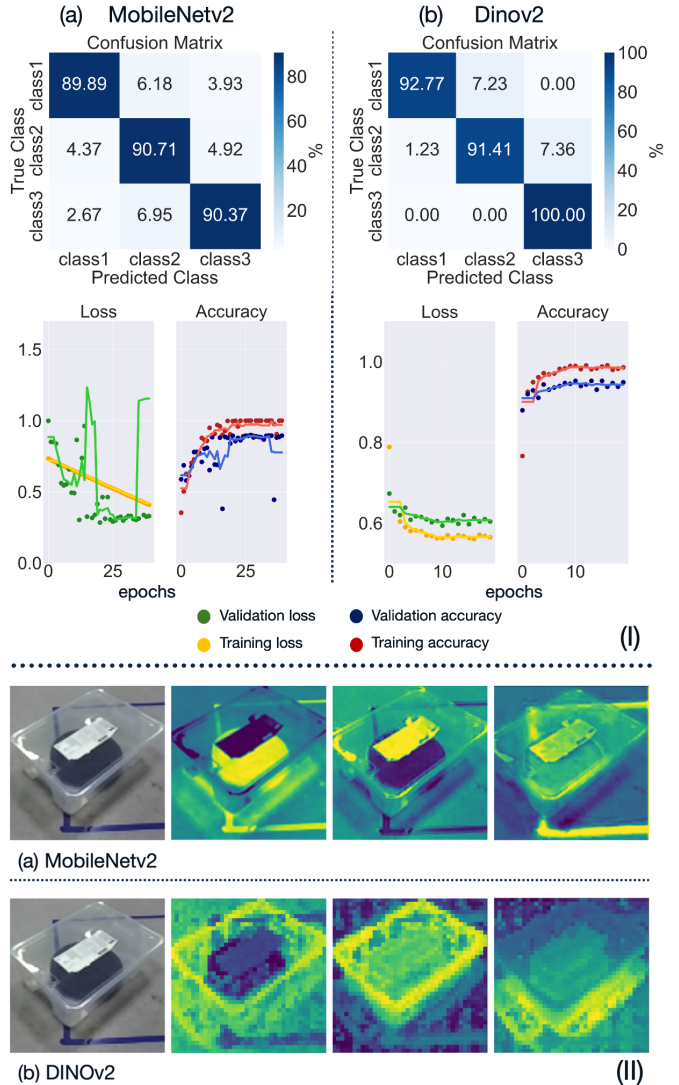


Fig. 5: Training history and performance of the payload estimation models (I). Comparison of features extracted by MobileNet2 and DINOv2 (II).

box). In contrast, DINOv2 effectively segmented foreground and background, as seen in its feature maps, and demonstrated depth estimation by assigning distinct gradients to pixels based on their distance from the observer. To further support these insights, we conducted a deeper analysis of DINOv2 extracted features across 20 input images, detailed in the supplementary material and accompanying code. This analysis included K-means clustering to examine similarities within feature maps across different inputs. Our findings show that DINOv2 consistently assigns similar features to similar objects, such as the background, boxes, box edges, and weights inside the boxes. Each of the three feature maps reveal distinct perception capabilities: channel 1 captures background-foreground separation and object detection, channel 2 exhibits strong depth perception, and channel 3 focuses on detecting weights inside the boxes. We speculate that the final attention block and MLP in our architecture integrate these features, enabling more precise payload categorization based on shape, content, and contextual cues. We attribute DINOv2s superior performance to its Transformer-based architecture, which enhances contextual understanding, and its unsupervised learning approach, which produces robust feature representations. This combination allows DINOv2 to outperform state-of-the-art CNNs in detailed object recognition and segmentation tasks. These results drive our choice to use DINOv2 for our real-time experiments.

C. Pipeline Validation

As outlined in Section III-B, during experiments we measure muscular activity to be compared with no-exoskeleton condition, we track output classifications of the pipeline, and ensure that each classification is correct only if the correct output of the classification is provided before the lifting cycle starts. We also collect human feedback on discomfort and preference similarly to what was done for baseline experiments to build validation functions. As shown in Figure 3 (II-a), regarding back muscle activation, we observed unexpected changes under the low weight condition, even though the light assistance selected by the pipeline should be the same as the one provided during the static assistance test. Improvements in the case of adaptive control are registered ($4.90 \rightarrow 11.07\%$ for mean and $8.35 \rightarrow 19.22\%$ for peak activation), which we attribute to reduced overall effort during the test, and some

light weight misclassification leading to stronger support. A strong improvement is registered for the medium and high weight conditions, where adapting the control to the handled weight strongly improves muscular activation reduction compared to static control condition ($9.13 \rightarrow 18.89\%$ for mean and $9.62 \rightarrow 23.05\%$ for peak activation for medium weight and $12.15 \rightarrow 20.68\%$ for mean and $9.99 \rightarrow 19.05\%$ for peak activation for heavy weight). We obtain similar results in terms of gradients when combining all of the muscles contributions together. We achieve instead a particularly interesting result when considering leg muscles, which also experience a decrease in peak ($-12.35 \rightarrow 1.08\%$ for medium weight) and mean ($-19.33 \rightarrow -2.65\%$ for medium weight) muscle activation when using an adaptive control compared to a static one during lifting. Overall, adaptive control shows strong improvements in EMG reduction across all the muscles. In alignment with baseline tests, D-VRF suggests an increase in perceived discomfort going towards adaptive control, especially marked for medium and heavy weights, while remaining almost unchanged when handling a light weight. This is a result aligned with baseline results, where stronger support led to increased perceived discomfort. P-VRF also aligns with results obtained from the baseline experiments: despite the discomfort slightly increasing, subjects still prefer higher assistance for higher weights, leading to preferring adaptive control compared to static one. Finally, all the T-VRF display gradients pointing towards adaptive control per each of the payload conditions. In conclusion, 83.33% of the subjects agreed in feeling safe letting the exoskeleton autonomously decide which control to select. Figure 6 shows the final validation performances of the pipeline in terms of confusion matrix and accuracies per each subject test and average final value. During real-time tests, the pipeline achieves 85.30%, 76.30% and 86.10% precisions for the light, medium, and heavy weight classes respectively, and an overall 82.41% accuracy. Overall, the pipeline shows balance between overestimations and underestimations of the weights, suggesting that no particular bias is present.

V. DISCUSSION

A. Exoskeleton Optimization Space and Contributions

Results in Section IV-A and Figure 3 (I) indicate that different support modulation strategies can optimize distinct performance metrics. For instance, maintaining high support effectively reduces both peak and mean back muscle activation. However, this approach increases peak activation in leg muscles, particularly during light-weight lifting. While not extensively documented, some research has indicated a comparable pattern, wherein the energy imparted by a non-grounded back exoskeleton seems to distribute throughout the body, possibly reducing back muscle engagement but also, under specific conditions, slightly altering leg loading [41], [42]. Given the negative impact on peak leg muscle activation when using strong support for light weight, an optimal approach for minimizing overall muscular effort would involve high support for reducing mean activation and lower support to mitigate peak activation. Alternatively, considering

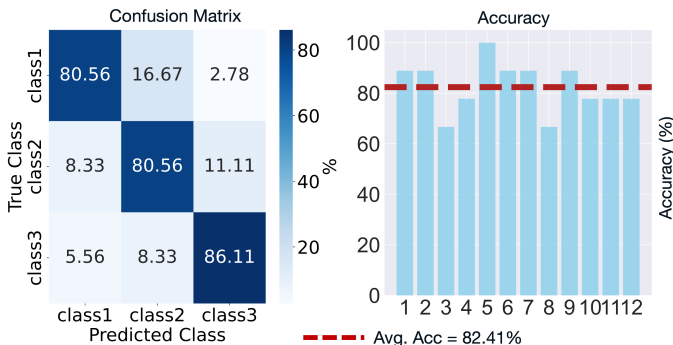


Fig. 6: Pipeline classification performances in terms of confusion matrix and subject-specific average accuracies.

back and leg muscle activity optimization separately, the best strategy would involve increasing support progressively with weight, from low to strong, ensuring a stable reduction in leg muscle activation. Regarding discomfort, results show that increasing support, regardless of payload, leads to higher perceived discomfort. This finding is consistent with our experience and participants' feedback, which suggest that greater support exacerbates joint misalignment, increases human-exoskeleton contact forces, and restricts natural movement, all contributing to discomfort. Comments gathered during experiments highlight that strong assistance made bending down more challenging, worsened joint misalignment, and caused localized pressure, particularly at anchoring points such as the thighs and shoulders. Nonetheless, user preference indicates a tendency to favor strong support for heavy loads and low support for lighter ones. This likely stems from a perceived benefit: for short-duration tasks like single-cycle lifting, the exoskeletons back muscle relief outweighs the discomfort, whereas for light loads, users do not find the additional support necessary, so they prefer to prioritize discomfort minimization. Once again, the preference function suggests that adaptive support is the most effective strategy. In the case of T-ORF, the support modulation trend is evident across all EMG-ORF contributions, highlighting that maintaining a static support level is suboptimal for maximizing EMG reduction, minimizing discomfort, and aligning with user preferences. Instead, an adaptive control strategy adjusting support from light to strong based on weight would yield the best overall performance. To the best of the authors' knowledge, this is the only study that considers multiple metrics in the effort to optimize exoskeleton performance.

B. Payload Estimation Models and Importance of Computer Vision-Based Techniques to Beat Latency

Our results in Section IV-B confirm that payload estimation from transparent boxes remains a challenging task. Despite achieving high accuracy (90.32 – 94.72%), factors such as varying viewpoints, light reflections, and occlusions caused by box shapes can still lead to misclassification. The MobileNetv2-based model exhibits unstable learning curves, raising concerns about its real-time reliability, even though the final epoch achieves high validation accuracy. Conversely, state-of-the-art Vision Transformer (ViT) architectures like DINOv2 demonstrate more stable training (Figure 5-I) and superior overall performance. While it is less pronounced in DINOv2, both models exhibit some degree of overfitting. However, since our objective is not to develop a zero-shot payload estimation model and industrial environments are typically standardized, training on a dataset collected within the same setting minimizes the risk of encountering vastly different objects, making this overfitting effect acceptable. Feature learning from raw images has been central to deep learning-based computer vision, particularly in CNN applications [43], [44]. However, ViT architectures, especially those trained in an unsupervised manner, have shown superior general feature extraction capabilities, outperforming CNNs in various applications. Our findings further support this, as

feature map analysis confirms that DINOv2 extracts higher-quality features, enabling more advanced image detection, segmentation, and depth perception capabilities that standard CNNs, even optimized ones, struggle to achieve. Figure 5-II illustrates how these advantages allow the DINOv2-based model to distinguish foreground from background, filter out irrelevant elements such as floor markings and labels, and demonstrate depth perception crucial for volume and shape estimation. These advanced capabilities result in correct classifications for DINOv2, while MobileNetv2 more frequently misclassifies objects. Real-time evaluations confirm strong performance. As shown in Figure 6, the system achieves a mean accuracy of 82.41%, with subject-specific accuracies closely distributed around this mean, indicating that our approach effectively mitigates the subject-specific variability found in other payload estimation methods [23]. Accuracy drops for subjects 3 and 8 are primarily due to communication conflicts between the cloud computing platform and the embedded Raspberry Pi, arising from interference between the embedded computer and the EMG wireless sensor system, both operating at the same frequency. While this highlights a limitation in our pipeline, it also suggests that improved system design could further enhance stability and accuracy. Additionally, the confusion matrix shows that misclassifications are evenly distributed around the diagonal, indicating a well-balanced model without inherent bias. All correctly classified transitions occurred before the lifting cycle began, ensuring prompt detection and support modulation. To the best of our knowledge, this is the only technique available to date that enables payload estimation and support modulation in advance, maximizing exoskeleton effectiveness and benefits. Our results in Figure 3 (II), particularly in terms of EMG-VRF, strongly support this claim.

C. The Importance of Adaptive vs Static Control

Results in Section IV-C indicate that, except when optimizing solely for discomfort, adaptive assistance is consistently preferred. Figure 3 (II) shows that adaptive control enhances EMG reduction across all contributions, even in cases where support levels should theoretically be the same, such as for light weights, where both static and adaptive assistance provide low support. An interesting finding is the increase in peak and mean leg muscle activation observed during experiments, particularly for the light-weight static assistance condition, which slightly deviates from baseline results. In addition to the pipeline's non-perfect classifications, we attribute this to differences in test protocols: while baseline tests involved controlled, standardized stoop lifting, validation tests allowed participants to move freely, lifting at their preferred speed and with their preferred style. As a result, some subjects performed a mixed stoop-squat lifting motion, leading to increased leg muscle activation. Video analysis and EMG data confirm this effect, particularly for subjects 2 and 8. This effect suggests that adaptive control allows subjects to lift weights more comfortably without relying on leg muscles, leading to greater muscle activity reduction in both the back and legs. For payload increasing static support does not substantially enhance muscle activity reduction, whereas adaptive support does, as

expected, by dynamically adjusting support based on payload. This trend is evident across all contributions. Regarding discomfort, the VRF results align with expectations, showing an increase under adaptive control. This supports the baseline findings that higher support levels lead to greater discomfort, as adaptive control adjusts assistance based on payload, while static support maintains low assistance regardless of weight. Similarly, the preference VRF indicates that most subjects favored adaptive control, as it provided greater support for heavier loads while minimizing discomfort for lighter ones by adapting to low assistance. When considering all factors together, the T-VRF results reveal a clear trend favoring adaptive control for performance optimization, validating the hypotheses drawn from baseline experiments. Eventually, our findings support the claim that adaptive control is necessary for performance optimization, suggesting a preference for active exoskeletons over passive ones.

D. Limitations & Future Work

Our pipeline shows promising results in real-time detection and validation, demonstrating that adaptive control can significantly improve performance. However, it has limitations that may hinder adoption in industrial settings. A key constraint is its reliance on transparent boxes, which aid detection and contextual inference. Estimating payloads in opaque boxes is more challenging, as even humans struggle without prior knowledge. In environments with known object weights (e.g., cataloged), the payload estimation layer can be bypassed, but alternative approaches, such as sensor fusion, are needed when a catalog is unavailable. Future work will explore continuous payload estimation by integrating EMG/FSM data for refinement in critical scenarios. Another limitation is that our method has only been tested in a controlled laboratory setting with young subjects. Future research should evaluate the pipeline in diverse industrial environments with real workers. Additionally, our pipeline currently runs on the cloud, which aligns with the Industry 5.0 paradigm but limits system independence and introduces potential real-time issues, such as communication delays. Future work should focus on optimizing hardware and software to enable embedded execution without increasing the exoskeleton's bulk.

VI. CONCLUSION

In this research, we addressed two key questions: identifying optimization spaces for back exoskeletons to determine optimal operating areas and exploring control adaptation strategies to enhance performance through exoskeleton context awareness. We established a two-dimensional optimization space using Optimization and Validation Representation Functions based on EMG reduction, perceived discomfort, and user preference. Experiments with 12 subjects revealed optimal operating regions, demonstrating that support modulation is essential for performance optimization. Building on these insights, we developed a computer vision-based adaptive control pipeline. Unlike previous approaches, our method is subject-independent, does not increase exoskeleton bulk, and minimizes latency by estimating payloads before

lifting. Integrated into the exoskeleton control and validated with 12 subjects, the pipeline demonstrated strong real-time accuracy and effectiveness across performance metrics. Our findings highlight the importance of adaptive control in optimizing exoskeleton performance and suggest that active exoskeletons could be preferred over passive/static ones to achieve the necessary adaptability. These results pave the way for further research in back exoskeleton optimization, context awareness, and high-level control adaptation.

DATA & CODE AVAILABILITY STATEMENT

This article has downloadable data available at [10.5281/zenodo.15125114](https://doi.org/10.5281/zenodo.15125114), provided by the authors. Further supplementary material on pipeline development details and shared code can be found at the following GitHub repository: [GitHubRepository](#).

CONFLICT OF INTERESTS

The authors declare that M.G. and F.B. hold shares in AGADE srl and AllyArm srl, and there were no further competing interests in the development of this research.

REFERENCES

- [1] A. Van der Have, S. Van Rossum, and I. Jonkers, "Squat lifting imposes higher peak joint and muscle loading compared to stoop lifting," *Applied Sciences*, vol. 9, p. 3794, 2019. [Online]. Available: <https://doi.org/10.3390/app9183794>
- [2] M. A. P. Dolan, "Repetitive lifting tasks fatigue the back muscles and increase the bending moment acting on the lumbar spine," *Journal of Biomechanics*, vol. 31, pp. 713–721, 1998.
- [3] B. P. Bernard and V. Putz-Anderson, "Musculoskeletal disorders and workplace factors: a critical review of epidemiologic evidence for work-related musculoskeletal disorders of the neck, upper extremity, and low back," *DHHS publication (NIOSH)*, pp. 97–141, 1997.
- [4] M. P. De Looze, T. Bosch, F. Krause, K. S. Stadler, and L. W. OSullivan, "Exoskeletons for industrial application and their potential effects on physical work load," *Ergonomics*, p. 671681, 2016.
- [5] S. Ding, F. A. Reyes, S. Bhattacharya, A. Narayan, S. Han, O. Seyram, and H. Yu, "A novel back-support exoskeleton with a differential series elastic actuator for lifting assistance," *IEEE Transactions on Robotics*, vol. 40, pp. 1327–1338, 2024.
- [6] J. Chung, D. Quirk, and M. e. a. Applegate, "Lightweight active back exosuit reduces muscular effort during an hour-long order picking task," *Commun Eng*, vol. 3, no. 35, 2024. [Online]. Available: <https://doi.org/10.1038/s44172-024-00180-w>
- [7] L. Roveda, L. Savani, S. Arlati, T. Dinon, G. Legnani, and L. Molinari Tosatti, "Design methodology of an active back-support exoskeleton with adaptable backbone-based kinematics," *International Journal of Industrial Ergonomics*, vol. 79, p. 102991, 2020. [Online]. Available: <https://www.sciencedirect.com/science/article/pii/S0169814120301682>
- [8] S. Toxiri, A. Calanca, J. Ortiz, P. Fiorini, and D. G. Caldwell, "A parallel-elastic actuator for a torque-controlled back-support exoskeleton," *IEEE Robotics and Automation Letters*, vol. 3, no. 1, pp. 492–499, 2018.
- [9] J. I. Kim, J. Choi, J. Kim, J. Song, J. Park, and Y.-L. Park, "Bilateral back extensor exosuit for multidimensional assistance and prevention of spinal injuries," *Science Robotics*, vol. 9, no. 92, p. eadk6717, 2024. [Online]. Available: <https://www.science.org/doi/abs/10.1126/scirobotics.adk6717>
- [10] A. Dal Prete, M. Gandolla, G. Andreoni, and F. Braghin, "Low Back Exoskeletons in Industry 5.0: From Machines to Perceiving Co-Pilots A State-of-the-Art Review," *Sensors*, vol. 25, p. 1958, 2025. [Online]. Available: <https://doi.org/10.3390/s25071958>
- [11] T. e. a. Walter, "Active exoskeleton reduces erector spinae muscle activity during lifting," *Frontiers in bioengineering and biotechnology*, vol. 11, p. 1143926, 2023.
- [12] T. Luger, M. Br, R. Seibt, M. A. Rieger, and B. Steinhilber, "Using a back exoskeleton during industrial and functional task effects on muscle activity, posture, performance, usability, and wearer discomfort in a laboratory trial," *Human Factors*, vol. 65, no. 1, pp. 5–21, 2023, pMID: 33861139. [Online]. Available: <https://doi.org/10.1177/00187208211007267>

- [13] K. A. Ingraham, C. D. Remy, and E. J. Rouse, "The role of user preference in the customized control of robotic exoskeletons," *Science Robotics*, vol. 7, no. 64, p. eabj3487, 2022. [Online]. Available: <https://www.science.org/doi/abs/10.1126/scirobotics.abj3487>
- [14] A. Ali, V. Fontanari, W. Schmoelz, and S. K. Agrawal, "Systematic review of back-support exoskeletons and soft robotic suits," *Frontiers in Bioengineering and Biotechnology*, vol. 9, 2021. [Online]. Available: <https://www.frontiersin.org/journals/bioengineering-and-biotechnology/articles/10.3389/fbioe.2021.765257>
- [15] M. e. a. von Arx, "From Stoop to Squat: A Comprehensive Analysis of Lumbar Loading Among Different Lifting Styles," *Frontiers in bioengineering and biotechnology*, vol. 9, p. 769117, 2021.
- [16] L. Mateos, "Characterizing lifting and lowering activities with insole for sensors in industrial exoskeletons," 06 2017.
- [17] E. S. Matijevich, P. Volgyesi, and K. E. Zelik, "A Promising Wearable Solution for the Practical and Accurate Monitoring of Low Back Loading in Manual Material Handling," *Sensors* 21, vol. 2:340, 2021.
- [18] M. Lazzaroni, T. Poliero, M. Sposito, S. Toxiri, D. G. Caldwell, C. Di Natali, and J. Ortiz, "Back-Support Exoskeleton Control Strategy for Pulling Activities: Design and Preliminary Evaluation," *Designs* 5, vol. 3:39, 2021.
- [19] M. e. a. Lazzaroni, "Acceleration-based Assistive Strategy to Control a Back-support Exoskeleton for Load Handling: Preliminary Evaluation," *IEEE 16th International Conference on Rehabilitation Robotics (ICORR), Toronto, ON, Canada*, vol. 625:360, 2019.
- [20] S. e. a. Toxiri, "Rationale, Implementation and Evaluation of Assistive Strategies for an Active Back-Support Exoskeleton," *Frontiers in robotics and AI*, vol. 5 53, 2018.
- [21] M. Ul Islam and S. Bai, "Payload estimation using force myography sensors for control of upper-body exoskeleton in load carrying assistance," *Modeling, Identification and Control: A Norwegian Research Bulletin*, vol. 40, pp. 189–198, 01 2019.
- [22] A. Tahir, Z. An, S. Bai, and M. Shen, "Robust payload recognition based on sensor-over-muscle-independence deep learning for the control of exoskeletons," *IEEE Transactions on Circuits and Systems II: Express Briefs*, vol. 70, no. 9, pp. 3699–3703, 2023.
- [23] Z. G. Xiao and C. Menon, "A review of force myography research and development," *Sensors (Basel, Switzerland)*, vol. 19, no. 20, p. 4557, 2019.
- [24] M. Pesenti, G. Invernizzi, and J. e. a. Mazzella, "IMU-based human activity recognition and payload classification for low-back exoskeletons," *Sci Rep* 13, vol. 1184, 2023.
- [25] O. A. M. F., R. Parameswari, C. Di Natali, D. G. Caldwell, and J. Ortiz, "Assessment and benchmarking of xonli: a natural language processing interface for industrial exoskeletons," pp. 3333–3340, 2024.
- [26] GPy, "GPy: A gaussian process framework in python," <http://github.com/SheffieldML/GPy>, since 2012.
- [27] C. E. Rasmussen and C. K. I. Williams, *Gaussian Processes for Machine Learning*. The MIT Press, 2006.
- [28] A. Dosovitskiy, L. Beyer, A. Kolesnikov, D. Weissenborn, X. Zhai, T. Unterthiner, M. Dehghani, M. Minderer, G. Heigold, S. Gelly, J. Uszkoreit, and N. Houlsby, "An image is worth 16x16 words: Transformers for image recognition at scale," 2021. [Online]. Available: <https://arxiv.org/abs/2010.11929>
- [29] J. Redmon, S. Divvala, R. Girshick, and A. Farhadi, "You only look once: Unified, real-time object detection," 2016. [Online]. Available: <https://arxiv.org/abs/1506.02640>
- [30] L. Yang, B. Kang, Z. Huang, Z. Zhao, X. Xu, J. Feng, and H. Zhao, "Depth anything v2," 2024. [Online]. Available: <https://arxiv.org/abs/2406.09414>
- [31] R. Ranftl, K. Lasinger, D. Hafner, K. Schindler, and V. Koltun, "Towards robust monocular depth estimation: Mixing datasets for zero-shot cross-dataset transfer," *IEEE Transactions on Pattern Analysis and Machine Intelligence*, vol. 44, no. 3, 2022.
- [32] M. Sandler, A. Howard, M. Zhu, A. Zhmoginov, and L.-C. Chen, "Mobilenetv2: Inverted residuals and linear bottlenecks," 2019. [Online]. Available: <https://arxiv.org/abs/1801.04381>
- [33] M. Caron, H. Touvron, I. Misra, H. Jgou, J. Mairal, P. Bojanowski, and A. Joulin, "Emerging properties in self-supervised vision transformers," 2021. [Online]. Available: <https://arxiv.org/abs/2104.14294>
- [34] T. Darcet, M. Oquab, J. Mairal, and P. Bojanowski, "Vision transformers need registers," 2023.
- [35] M. Oquab, T. Darcet, T. Moutakanni, H. Vo, M. Szafraniec, V. Khalidov, P. Fernandez, D. Haziza, F. Massa, A. El-Nouby, M. Assran, N. Ballas, W. Galuba, R. Howes, P.-Y. Huang, S.-W. Li, I. Misra, M. Rabbat, V. Sharma, G. Synnaeve, H. Xu, H. Jegou, J. Mairal, P. Labatut, A. Joulin, and P. Bojanowski, "Dinov2: Learning robust visual features without supervision," 2024. [Online]. Available: <https://arxiv.org/abs/2304.07193>
- [36] PatrickLabatut, "facebookresearch/dinov2," <https://github.com/facebookresearch/dinov2>, 2024, accessed: 2025-01-22.
- [37] S. A. Julious, "Sample size of 12 per group rule of thumb for a pilot study," *Pharmaceutical Statistics*, vol. 4, no. 4, pp. 287–291, 2005. [Online]. Available: <https://onlinelibrary.wiley.com/doi/abs/10.1002/pst.185>
- [38] S. Project, *Surface Electromyography for the Non-Invasive Assessment of Muscles (SENIAM) - Recommendations for Sensor Placement*, accessed: 2025-01-15. [Online]. Available: <https://www.seniam.org/>
- [39] P. Konrad, *The ABC of EMG: A Practical Introduction to Kinesiological Electromyography*. Scottsdale, AZ: Noraxon INC, April 2005, version 1.0, April 2005.
- [40] G. E. P. Box, J. S. Hunter, and W. G. Hunter, *Statistics for Experimenters: Design, Innovation, and Discovery*, 2nd ed. Wiley, May 2005.
- [41] D. M. Frost, M. Abdoli-E, and J. M. Stevenson, "Plad (personal lift assistive device) stiffness affects the lumbar flexion/extension moment and the posterior chain emg during symmetrical lifting tasks," *Journal of Electromyography and Kinesiology*, vol. 19, no. 6, pp. e403–e412, 2009. [Online]. Available: <https://www.sciencedirect.com/science/article/pii/S1050641108002034>
- [42] T. Luger, M. Br, R. Seibt, M. A. Rieger, and B. Steinhilber, "Using a back exoskeleton during industrial and functional task effects on muscle activity, posture, performance, usability, and wearer discomfort in a laboratory trial," *Human Factors*, vol. 65, no. 1, pp. 5–21, 2021. [Online]. Available: <https://doi.org/10.1177/00187208211007267>
- [43] A. Voulodimos, N. Doulamis, A. Doulamis, and E. Protopapadakis, "Deep learning for computer vision: A brief review," *Computational Intelligence and Neuroscience*, vol. 2018, p. 7068349, 2018, pMID: 29487619, ISSN: 1687-5273 (Electronic), 1687-5265 (Print). [Online]. Available: <https://doi.org/10.1155/2018/7068349>
- [44] D. Beaglehole, A. Radhakrishnan, P. Pandit, and M. Belkin, "Mechanism of feature learning in convolutional neural networks," 2023. [Online]. Available: <https://arxiv.org/abs/2309.00570>